Clays and Clay Minerals, Vol. 51, No. 2, 121–132, 2003.

A CRYSTAL-CHEMICAL STUDY OF NATURAL AND SYNTHETIC ANIONIC CLAYS

CRISTINA DE LA CALLE[1], CHARLES-HENRI PONS[1], JACQUES ROUX[1] AND VICENTE RIVES[2]

[1] ISTO, UMR 6113, CNRS-Université d'Orléans, 1A Rue de la Ferollerie, 45071 Orleans Cedex 2, France,
[2] Departamento de Química Inorgánica, Universidad de Salamanca, 37008 Salamanca, Spain

Abstract—A comparative crystallochemical study was performed on natural and synthetic hydrotalcite-like compounds with similar compositions. The nature of the brucite-like sheet stacking was addressed by means of powder X-ray diffraction. From the resulting electron diffraction patterns it was possible to establish the order-disorder of the cations in the brucite-like sheet. The results show that a natural sample from Snarum is an intergrowth of hydrotalcite ($3R_1$ polytype) and manasseite ($2H_1$ polytype) at a ratio of 77:23 (wt.%). An aluminian serpentine is associated with the hydrotalcite and manasseite minerals. The structure of a synthetic sample, Mg:Al = 2:1, was determined as space group $R\bar{3}m$. For a few crystals in this sample, the octahedral cation distribution is compatible with the observed supercell ($a = a'\sqrt{3}$). A second synthetic sample showed the presence of stacking faults and was described as a random layer sequence of two polytypes (3*R* and 2*H*).

Key Words—Anionic Clays, Crystal Structure, Hydrotalcite-like Group, Polytype, Snarum, Stacking Faults, Synthetic Double Hydroxides, X-ray Diffraction.

INTRODUCTION

An anionic clay is mainly defined by its chemical composition with the general formula $[M^{II}_{1-x}M^{III}_x(OH)_2][X^{m-}_{x/m}]nH_2O$, and by two important structural features: the basal spacing d_{001}, and the layer sequence. The term 'anionic clay' refers to the better known cationic clays, layered aluminosilicates formed by negatively charged layers where the electric charge is balanced by exchangeable, hydrated cations located between the layers. The anionic clays are also known as layered double hydroxides (LDHs) and include members of the hydrotalcite-manasseite group.

The present paper is concerned with a comparative crystallochemical study of one natural and two synthetic samples of these anionic clays. Special attention is paid to the study of polytypism, *i.e.* the stacking arrangement of the brucite-like sheets in the different samples, as well as to the cation (Mg, Al) distribution within the brucite-like sheets discussed in correlation to the chemical composition.

The first natural mineral belonging to this family of anionic clays was discovered in Sweden in 1842, and was given the general formula $Mg_6Al_2(OH)_{16}CO_3.4H_2O$. Most of the early studies on synthesis, stability, solubility and structure were carried out by Feitknecht (1930). A paper reviewing the structural studies, published by Frondel (1941), clearly recognized the hexagonal and rhombohedral forms.

Feitknecht (1953) described the structure of these anionic clays as similar to the so-called 'cadmium iodide (CdI_2)' structure. This structure consists of a hexagonal close packing of OH groups with the metal cations (Mg or Al) filling all the octahedral holes every two interlayers. This unit, formed by a plane of OH groups, a metal cation plane and a second OH plane, is known as a 'brucite-like sheet', as this is the base structure of $Mg(OH)_2$. Upon Mg-Al substitution, the brucite-like sheet becomes positively charged, the charge being balanced by anions located between the brucite-like sheets, together with water molecules. The unit-cell of hydrotalcite-like minerals may consist of several brucite-like sheets producing crystals of different polytypes and it is possible to classify polytypes based on the number of brucite-like sheets in the unit-cell: the 1*H* polytype is formed by one brucite-like sheet per unit-cell; the 2*H* polytype is formed by two hexagonal brucite-like sheets, and the 3*R* polytype is formed by three brucite-like sheets with rhombohedral symmetry.

Such an approach misses important structural features associated with the stacking of brucite-like sheets. Booking and Drits (1993) found that neighboring layers may be stacked in two different ways, building two kinds of interlayers: P-type where OH planes lie one on top of the other forming prisms and O-type where OH groups form octahedra. All polytypes may be separated into three groups: homogeneous interlayers of O- or P-type, and alternating interlayers of both types.

The carbonate $[Mg_{1-x}Al_x(OH)_2]^{x+}[xX^-nH_2O]$, where X^- is $\frac{1}{2}CO_3^{2-}$, occurs in two dimorphic forms: rhombohedral hydrotalcite and hexagonal manasseite.

In the hydrotalcite structure the layers are stacked with rhombohedral symmetry (BC ... CA ... AB ... BC ...) for the brucite-like sheets (using the hydroxyl plane notation of Bookin and Drits, 1993) and three layers are present per unit-cell ($c = 3c' = 23.4$ Å); in the manasseite structure they are stacked with hexagonal symmetry (BC CB BC) and two brucite-like sheets are present per unit-cell ($c = 2c' = 15.6$ Å).

* E-mail address of corresponding author:
charles-henri.pons@univ- orleans.fr
DOI: 10.1346/CCMN.2003.0510201

The number of papers on anionic clays has increased in recent years because of their application in many different fields, mainly in water purification, medicine and as catalysts or catalyst precursors (Cavani *et al.*, 1991; Roy *et al.*, 1992; Szostak and Ingram, 1995; Rives and Ulibarri, 1999). These papers encouraged the present authors to study the relationship between structural and textural features and chemical compositions in these materials. We have studied three samples of different origins, one natural and two synthetic with different Mg:Al ratios (2:1 and 3:1).

In this work, the nature of the stacking was addressed by means of powder X-ray diffraction (XRD). Selected area electron diffraction (SAED) allowed us to establish the nature of the cation order in the brucite sheet. The textures of the materials were ascertained by transmission electron microscopy (TEM) and scanning electron microscopy (SEM). Elemental wet chemical analyses by atomic absorption, as discussed in reference to the electron diffraction and XRD results, demonstrated a relationship between the composition and the degree of order of the layer cations and between the composition and the stacking of the layers.

MATERIALS AND METHODS

Our study was performed on a natural sample (N1) from Snarum (Norway), obtained from Muséum des Sciences Naturelles de Paris (Galerie de Minéralogie, sample 68.302) and on two synthetic samples: a commercial specimen (sample S1), kindly supplied by Süd-Chemie (Germany), and material synthesized in our laboratory (sample S2) as described below. The compositions of the synthetic samples were close to that of the natural sample.

Mineralogical properties and origin of the sample from Snarum (sample N1)

Hydrotalcite is found in different deposits, *e.g.* in Snarum (South Norway), Chichine (Ural Montains), and Vezna (Czechoslovakia). The deposit in Snarum is located in Precambrian rocks west of Oslo , where other minerals are also found, *e.g.* serpentine, forsterite, hematite, *etc.* (Raade, 1970). In this deposit, milky-white hydrotalcite is associated with a greenish mineral; the hydrotalcite is easily scratched with a finger-nail, and it appears as greasy white masses. The specimen from Snarum comprised some 20 g of material, mostly in a single aggregate of flaky crystals in roughly parallel orientation.

In nature, hydrotalcite and manasseite are commonly found intergrown, manasseite generally forming the core and hydrotalcite the outer part of the grain. Thus, hydrotalcite seems to form later than manasseite, and probably at lower temperatures. For this reason, it is generally accepted that hydrotalcite is more easily synthesized than manasseite (Roy *et al.*, 1953; Gastuche et *al.*, 1967; Pausch *et al.*, 1986).

Synthesis of sample S2

Sample S2 was synthesized following the constant-pH method, using a Metrohm 691 pH meter connected to a 725 Dosimat automatic dispenser from Metrohm. A solution containing 0.5 mol $MgCl_2.6H_2O$ and 0.25 mol $AlCl_3.6H_2O$ dissolved in 250 mL of water was added drop wise (~30 drops/min) to an aqueous solution containing 1.7 mol NaOH and 0.5 mol Na_2CO_3 in 500 mL of water (all chemicals were from Panreac, Spain); the process was carried out at room temperature and the suspension was stirred magnetically. Once addition was completed, the mixture was stirred further at room temperature for 2 h. The suspension was heated gently at ~50ºC until the total volume was reduced to ~500 mL. The solid was filtered and washed until no traces of chloride or sodium ions were detected in the washing liquid.

Analysis of Al and Mg by atomic absorption

Elemental chemical analyses for Mg and Al were performed by atomic absorption (air-acetylene and N_2O, respectively) in a GB905AA spectrometer, after dissolving ~30 mg of sample with HF-HCl-H_3BO_3 in order to attain a relative precision close to 1% for the molar Al:Mg ratio. Standard reference materials were prepared in a matrix as similar as possible to the samples under analysis. The solutions were diluted to obtain concentrations in the optimum range for both elements (0.5–0.8 ppm for Mg and 80–100 ppm for Al). Generally, five standards of three to six solutions were analyzed in each experiment. In order to minimize the error originating from the drift in the instrument conditions (especially for Al with the acetylene-N_2O flame), three or five measurements were performed for each solution, alternating standards and unknown samples. A least-squares algorithm using absorbance ratio between each pair of consecutive measurements was used to minimize the effect of instrumental drift. The overall analytical uncertainty for the most difficult element (Al) was referenced to a standard mineral (albite) and found to be better than 1% (see reproducibility of measurements for sample S1 and for albite in Table 1).

X-ray diffraction

X-ray diffraction patterns were obtained using a Siemens D500 diffractometer in Bragg-Brentano reflection geometry with CuKα radiation (40 kV, 20 mA, Ni-filtered) recording at 2º2θ/min. The horizontal axis goniometer allowed patterns to be obtained between 5 and 110º2θ The slits had an opening of 1º and the receiving slit an opening of 0.15 mm. The synthetic samples were studied as unoriented powders, while one unground section was used for the natural sample. In fact, the natural sample is an intergrowth of hydrotalcite and manasseite. To improve the resolution of the XRD pattern and to identify and quantify the two phases

https://doi.org/10.1346/CCMN.2003.0510201 Published online by Cambridge University Press

Table 1. Elemental chemical analysis for Mg and Al. Structural formulae.

Sample	Amount of solid (mg)	Weight of solution (g)	[Al] (ppm)	Weight fraction of Al	[Mg] (ppm)	Mg/Al Molar ratio
Snarum N 1	30.00	43.96	55.01	0.0806	151.8	3.06
Synthetic S1	30.20	39.86	81.60	0.1077	149.0	2.02
Synthetic S1	31.30	43.18	78.55	0.1084	147.6	2.08
Synthetic S2	42.70	49.55	78.95	0.0916	223.0	3.13
Albite	34.55	43.33	82.35	0.1033		

Sample	Structural formulae	Mg/Al ratio
Snarum N1	$[Mg_{6.03}Al_{1.97}(OH)_{16}](CO_3)_{0.985}.7.5H_2O$	3.06:1
Synthetic S1	$[Mg_{5.38}Al_{2.62}(OH)_{16}](CO_3)_{1.31}.5.6H_2O$	2.05:1
Synthetic S2	$[Mg_{6.07}Al_{1.93}(OH)_{16}](CO_3)_{0.965}.2.2H_2O$	3.13:1

correctly, a ground Snarum sample was introduced into the capillary and also studied using a goniometer with $CoK\alpha_1$ and a curved positive sensitive detector (INEL CPS 120). This detector allowed the pattern to be obtained between 5 and 120°2θ The vertical axis goniometer was used in Debye-Scherrer geometry. The X-ray beam was focused by reflection on the (101) planes of a quartz crystal with a radius of curvature of 1400 mm and cut at 8° (Johann-type cut). This quartz crystal monochromator is located just behind the X-ray tube. The monochromatic beam converges in the horizontal plane and slightly diverges in the vertical plane. Calibration software is used to reduce the deviation of the linear calibration introduced by the delay line (Roux and Volfinger, 1996). Structure determination of the Snarum and S1 samples was performed with the RIETICA Rietveld program (Hunter and Howard, 2000).

Electron microscopy

Study by TEM. A JEOL CX TEMSCAN microscope was used, with a point-to-point resolution of 7 Å and an accelerating potential of 100 kV. The morphology of isolated stacks of the different samples was studied, as well as the SAED patterns along [00*l*].

Study by SEM. We used an Hitachi S 4200 Field Emission Gun SEM with Si (Li) detectors from Oxford Link Isis, with a resolution of 136 eV. The images were obtained with a potential of 1 kV, and qualitative microprobe analyses were performed under a potential of 15 kV. The study included an analysis of the surface texture, shape and size of the sample crystallites (both natural and synthetic samples), as well as a cartographic determination of the main elements.

RESULTS

Structural formulae: elemental chemical analyses by atomic absorption

The results obtained for the samples studied are summarized in Table 1. From these, the structural formulae of the samples could be determined, assuming that: (1) a total of eight cations (Mg and Al) exist per formula; (2) there are 16 OH groups per formula; (3) the number of carbonate ions per formula in the interlayer equals one half of the number of Al cations; and (4) the amount of interlayer water depends on the ambient conditions and relative humidity. The calculated formulae are also included in Table 1. The amount of interlayer molecular water was determined from the

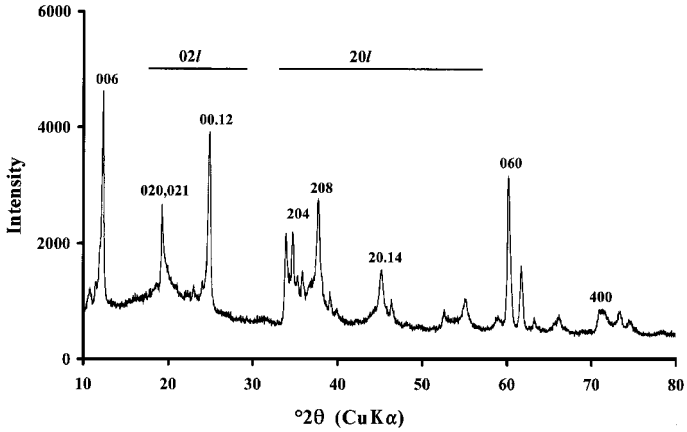

Figure 1. XRD pattern for the sample from Snarum (green part).

https://doi.org/10.1346/CCMN.2003.0510201 Published online by Cambridge University Press

Table 2. XRD data for the green part of the Snarum sample (serpentine).

hkl	d_{obs} (Å)	d_{calc} (Å)[1]	I_{obs}	I [2]
006	7.189	7.189	100	100
020,021	4.607	4.608, 4.581	41	35
026	3.850	3.879	6	5
027	3.702	3.690	6	5
00.12	3.579	3.595	80	100
200	2.655	2.663	15	15
202	2.642	2.642	41	55
203	2.613	2.618	25	22
204	2.584	2.585	41	40
205	2.530	2.544	20	15
206	2.485	2.497	23	35
207	2.443	2.444	10	15
208	2.383	2.387	58	80
209	2.303	2.327	15	10
20.10	2.250	2.266	7	15
20.14	2.004	2.015	26	30
20.15	1.955	1.954	13	10
310, 311, 312	1.739	1.743, 1.742, 1.737	9	5
20.20	1.665	1.676	15	15
31.12, 20.22	1.564	1.568, 1.579	7	10
060	1.536	1.536	70	65
066	1.502	1.502	28	10
400	1.328	1.331	12	10
06.18	1.290	1.293	10	10

[1] Orthogonal structure. $a = 5.32_5$ Å; $b = 9.21_6$ Å; $c = 43.13_4$ Å
[2] Gillery (1959): 6(3)-layer structure

stoichiometric formula and the weight fraction of Mg and Al determined by elemental chemical analysis. The amount of water calculated for the synthetic samples was similar to that found by other researchers (Bellotto *et al.*, 1996). In the natural sample, however, the number of molecules of water per unit-cell is higher and may vary with the relative humidity. Particle size also affects the quantity of water absorbed. If the results for the two synthetic samples (2.2 H_2O for S2 with 5.6 H_2O for S1) are compared, the relationship to particle size is obvious (see the later section on SEM and TEM). However, it is more difficult to interpret the results for the Snarum sample, which is an intergrowth of hydrotalcite-manasseite.

The results show that the amount of Al in the brucite-like sheet varied from sample to sample. In natural materials, the Mg:Al ratio was close to 3 (Brindley and Kikkawa, 1979), as in our natural sample N1. Sample S1 presented a Mg:Al ratio near 2, while sample S2 exhibited a ratio near 3, as in natural N1. Brindley and Kikkawa (1979) have seen in synthetic samples that the highest percentage of R^{3+} ions is near 33%, correspond-

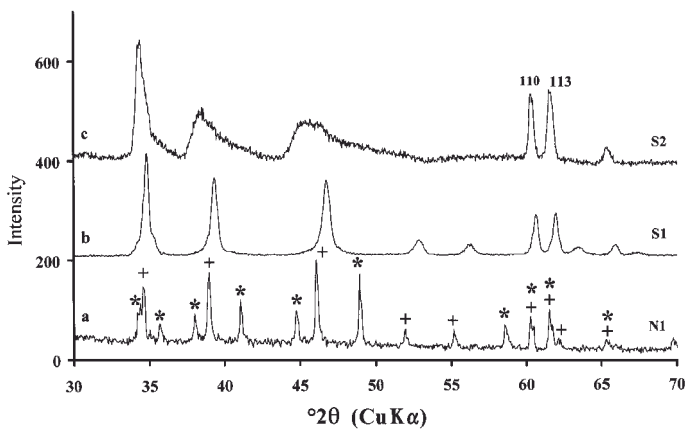

Figure 2. XRD patterns for the white part of the Snarum sample (a), the synthetic S1 sample (b) and the synthetic S2 sample (c). *: manasseite reflections, +: hydrotalcite reflections.

https://doi.org/10.1346/CCMN.2003.0510201 Published online by Cambridge University Press

ing to an R^{2+}:R^{3+} ratio of 2:1. The lowest limit is probably near 17–20% or a ratio of ~4:1 or 5:1. These results can be considered in relation to possible distributions of Al ions replacing Mg ions.

Crystal structure: X-ray and electron diffraction

Snarum serpentine. Figure 1 shows the XRD pattern of the green powder from Snarum, which indexes to a 6-layer serpentine (Gillery, 1959). Table 2 gives the X-ray powder data for this sample. That author investigated the substitution of Al for Mg and Si in serpentine by hydrothermal synthesis. Below 500ºC, aluminian lizardite is formed. Gillery found that lizardite-1*T* was the predominant polytype at the magnesian end of the system, but a 6-layer polytype increased in concentration as the Al substitution increased from $x = 0.25$ to $x = 1.00$ for the composition $(Mg_{3-x}Al_x)(Si_{2-x}Al_x)O_5(OH)_4$. Bailey and Tyler (1960) described a naturally occurring aluminian serpentine that gives a powder pattern similar to that of Gillery's synthetic 6-layer material. Shirozu and Momoi (1972) also synthesized this structure in the Mg-Al-Si system. They confirmed Gillery's observations that the amount of 6-layer lizardite increased at the expense of the 1-layer form with increasing Al substitution. By comparison with Gillery's diffraction data, we conclude that the green part of the Snarum sample is an aluminian lizardite designated as the 6(3) type because its strong reflections resemble those of a 3-layer orthorhombic (or 1-layer monoclinic) structure (Table 2). The reflection at 1.536 Å can be indexed as 060 with respect to the 1-layer monoclinic cell and *b* is 6 times d_{060}, *i.e.* 9.21_6 Å. The *a* parameter is deduced as 5.32_5 Å.

Selected area diffraction patterns, along *c**, are consistent with hexagonal symmetry.

Our XRD pattern reveals disordered stacking of layers along *b*, as shown by the mainly diffuse, 'tailed' reflections. The sequence of 02*l*, 11*l* reflections in the 20–30º2θ range is reduced to a simple asymmetry diffraction band with the superimposed 00.12 basal reflection (Drits and Tchoubar, 1990). In the 35–55º2θ range, discrete reflections with indices 13*l*, 20*l* occur and in the 60–65º2θ range, discrete reflections with indices of 06*l* appear. From considerations of the reflections with the index $k = 3n$ and with $k \neq 3n$ we can recognize the presence of random layer displacement of type *pb*/3, *p* being an integer. If displacements with different values of *p* occur randomly, then reflections with the index $k = 3n$ are unaffected and those with $k \neq 3n$ are weak or absent (Brindley, 1980; de la Calle *et al.*, 1988).

Snarum hydrotalcite and manasseite. The XRD pattern (CuKα radiation) of the unground section (white portion) of the Snarum sample is shown in Figure 2a. From data in Table 3, we can conclude that sample N1 is an intergrowth of manasseite ($2H_1$ polytype) and hydrotalcite ($3R_1$ polytype). As stated previously, the 3-layer polytype has P-type interlayers; the OH groups within the adjacent brucite-like sheets outline prisms in the interlayer and are denoted by an equal sign (=). The sequence is represented as ...AC=CB=BA=AC... and corresponds to space group $R\bar{3}m$. In a brucite-like sheet AC the lower surface of the brucite-like sheet is a plane of hydroxyls in which OH groups occupy *A* sites, cations fill octahedral positions and the upper surface is formed by OH groups in *C* sites. The polytype $2H_1$ has

Table 3. XRD data for the natural Snarum sample (white part = hydrotalcite and manasseite intergrown).

	Hydrotalcite [1]		
hkl	*d* (Å) calculated	*d* (Å) observed	º2θ CuKα calculated
003	7.800	7.786	11.33
006	3.900	3.901	22.78
101	2.633	n.o.	34.02
009	2.600	n.o.	34.47
012	2.585	2.587	34.68
104	2.414	n.o.	37.22
015	2.306	2.310	39.03
107	2.077	n.o.	43.54
018	1.964	1.968	46.18
00.12	1.950	n.o.	46.53
10.10	1.754	1.759	52.10
01.11	1.659	1.661	55.33
00.15	1.560	n.o.	59.17
110	1.530	1.533	60.45
113	1.501	1.505	61.73
10.13	1.489	1.490	62.30
116	1.424	1.427	65.47
01.14	1.414	n.o.	66.03

	Manasseite [2]		
hkl	*d* (Å) calculated	*d* (Å) observed	º2θ CuKα calculated
002	7.800	7.786	11.334
004	3.900	3.901	22.782
010	2.650	n.o.	33.795
011	2.613	2.610	34.294
006	2.600	n.o.	34.465
012	2.509	2.514	35.754
013	2.361	2.364	38.080
014	2.192	2.194	41.147
015	2.020	2.023	44.835
008	1.950	n.o.	46.532
016	1.856	1.859	49.042
017	1.706	n.o.	53.692
018	1.571	1.573	58.736
00.10	1.560	n.o.	59.175
110	1.530	1.533	60.455
112	1.501	1.505	61.731
019	1.451	n.o.	64.145
114	1.424	1.427	65.474
01.10	1.344	1.348	69.912

n.o. = not observed
Calculated: [1] hexagonal $a = 3.06$ Å, $c = 23.4$ Å
[2] hexagonal $a = 3.06$ Å, $c = 15.6$ Å

https://doi.org/10.1346/CCMN.2003.0510201 Published online by Cambridge University Press

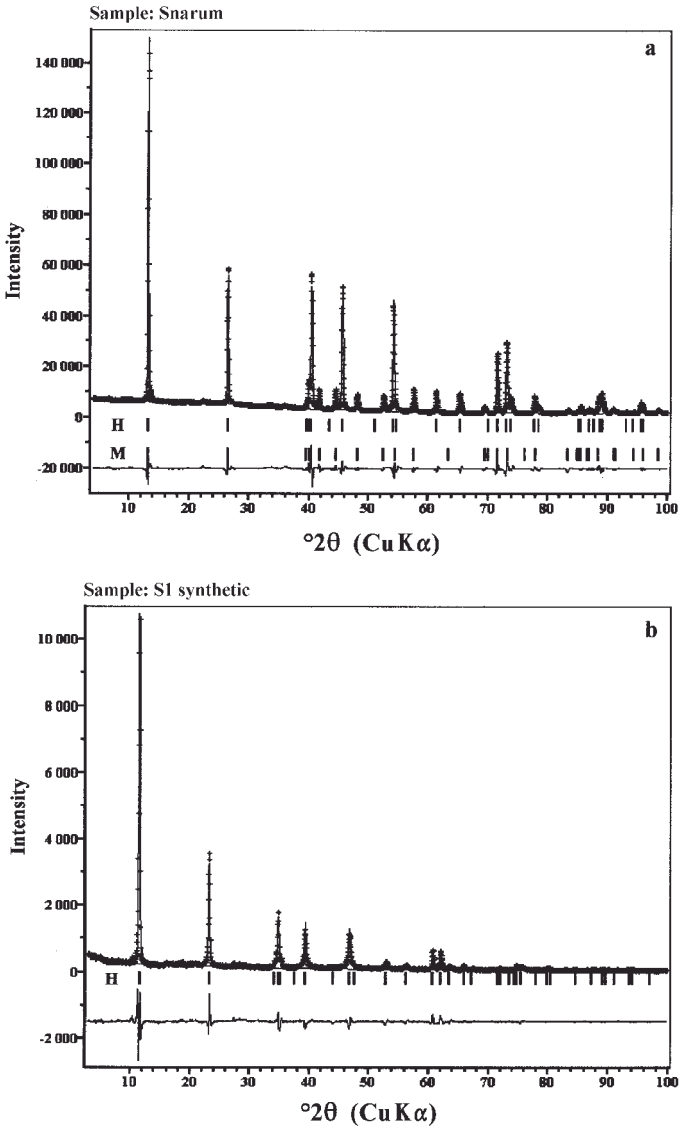

Figure 3. Experimental, calculated and difference X-ray powder patterns for the white part of the Snarum sample (a) and the synthetic S1 sample (b). H: hydrotalcite reflections, M: manasseite reflections.

hexagonal symmetry. This 2-layer polytype is represented by the sequence ...AC=CA=AC... and the space group corresponds to $P6_3/mmc$.

Thus, the Snarum sample was analyzed using space group $R\bar{3}m$ for the hydrotalcite phase and space group $P6_3/mmc$ for the manasseite (Allmann and Lohse, 1966). The experimental and calculated patterns are shown in Figure 3a. The site occupancies were fixed according to the nominal composition. The structural parameters and atomic positions are reported in Table 4, while the interatomic distances and angles are listed in Table 5. A single atomic displacement factor was refined and O (CO_3 + H_2O) and C were constrained to the z = 0.5 plane for the hydrotalcite phase and z = 0.25 plane for the manasseite phase. For the two phases the octahedra in the brucite-like sheet were shortened along c. The proportions of the hydrotalcite and manasseite phases in the Snarum sample have been determined as 77 wt.% and 23 wt.%, respectively.

Electron diffraction (Figure 4a) is consistent with hexagonal symmetry within the layer planes ($hk0$). There is no indication of any superlattice produced by an ordered distribution of the Mg and Al cations. In addition this sample exhibits good crystallinity and virtually no stacking faults as shown by the sharpness and symmetry of the 01l reflections (Bellotto *et al.*, 1996).

Synthetic sample S1. The XRD pattern of the synthetic S1 sample is shown in Figure 2b. The structure was determined with space group $R\bar{3}m$ in accord with previous studies of similar samples (Arakcheeva *et al.*, 1996; Bellotto *et al.*, 1996). This sample exhibits good

https://doi.org/10.1346/CCMN.2003.0510201 Published online by Cambridge University Press

Table 4. Rietveld results.

Sample	Snarum		S1
Phases	Hydrotalcite	Manasseite	Synthetic
Mg/Al	3.06	3.06	2.05
Space group	$R\bar{3}m$	$P6_3mmc$	$R\bar{3}m$
Unit-cell parameters (Å)	a = 3.0591(3)	a = 3.0571(2)	a = 3.0502(4)
	c = 23.377(1)	c = 15.598(2)	c = 22.925(3)
Statistical indices	R_{wp} = 0.13	R_{wp} = 0.13	R_{wp} = 0.20
Cell volume (Å^3)	189.5^3	126.3	184.7
Wt.%	77	23	100

Atomic positions: Snarum hydrotalcite phase

Atom	x	y	z	Site	Occupancy
Mg	0.0	0.0	0.0	3a	0.76
Al	0.0	0.0	0.0	3a	0.24
OH	0.0	0.0	0.3777(4)	6c	1
C	1/3	2/3	1/2	6c	0.061
O (CO_3+H_2O)	0.09(1)	−0.09(1)	1/2	18h	0.15

Atomic positions: Snarum manasseite phase

Atom	x	y	z	Site	Occupancy
Mg	0.0	0.0	0.0	2a	0.76
Al	0.0	0.0	0.0	2a	0.24
OH	1/3	2/3	0.0702(3)	4f	1
C	0.0	0.0	1/4	2b	0.12
O (CO_3+H_2O)	0.25(1)	0.50(1)	1/4	6h	0.31

Atomic positions: synthetic S1

Atom	x	y	z	Site	Occupancy
Mg	0.0	0.0	0.0	3a	0.67
Al	0.0	0.0	0.0	3a	0.33
OH	0.0	0.0	0.3799(5)	6c	1
C	1/3	2/3	0.5	6c	0.15
O (CO_3+H_2O)	0.09(1)	−0.09(1)	0.5	18h	0.64

crystallinity and virtually no stacking faults, as shown by the sharpness and symmetry of the 01l reflections and allows accurate Rietveld-type structural analysis to be performed. Peak broadening is inferred to result from small particles sizes.

The experimental and calculated patterns are shown in Figure 3b. The site occupancies have been fixed according to the nominal composition. The structural parameters and atomic positions are reported in Table 4 and the interatomic distances are listed in Table 5. As with the Snarum sample, a single atomic displacement factor was refined and O (CO_3 + H_2O) and C were constrained to the z = 0.5 plane. The octahedra in the brucite-like sheet are also flattened along c. The high

Table 5. Interatomic distances and angles.

Sample	Snarum		S1
Phases	Hydrotalcite	Manasseite	Synthetic
Interatomic distances (Å)			
(Mg,Al)–OH	2.049(2)	2.077(1)	2.060(4)
$(OH-OH)_{shared\ edges}$	2.726(4)	2.812(6)	2.770(2)
$(O-OH)_{layer\text{-}interlayer}$	2.897(1)	2.839(3)	2.792(1)
C–O	1.289(5)	1.323(1)	1.285(5)
Layer thickness	2.074	2.186	2.135
Interlayer thickness	5.716	5.613	5.515
Angles (°)			
OH–(Mg,Al)–OH	99.9(1)	97.0(2)	98.2(4)
OH–(Mg,Al)–OH	80.1(1)	83.0(2)	81.8(4)

https://doi.org/10.1346/CCMN.2003.0510201 Published online by Cambridge University Press

value of the R_{wp} (statistical agreement weighted factor) may indicate the presence of some stacking faults.

For a few crystals, SAED patterns with zone axis [00*l*] showed evidence of a superlattice (Figure 4b). This superlattice can be indexed with a = 5.32 Å ($\sqrt{3}$ times the primary a translation), and it may indicate the existence of regions in which the Mg and Al ions are ordered among octahedral sites. In light of the Mg:Al ratio of 2:1, several ordered configurations are possible. The supercell observed probably arises from small areas where an ordered distribution of cations appears. One should be cautious in deducing the existence of the superlattice throughout the sample. The proportion of crystals with a superstructure, detected by TEM, was in fact low for the sample as a whole. This is consistent with the PXRD, where a supercell with long-range order is not detected. Substitution of an Al ion for an Mg ion creates an excess local charge of +1. Therefore, Al cations are likely to avoid neighboring sites because of mutual repulsion. Figure 5 illustrates an arrangement of Mg and Al cations in the octahedral sheet that maintains a 2:1 Mg to Al ratio and satisfies Al avoidance principles. Each Al position is surrounded by six Mg positions, as was previously concluded in the study by Brindley and Kikkawa (1979) concerning the compatibility between Mg-Al substitutions and the distribution of cations in the octahedral sheet. This distribution corresponds to the largest value reported for Mg-Al substitution; the value here obtained for a ($a'\sqrt{3}$) is in agreement with the value reported by these authors. Gastuche *et al.* (1967) also reported superlattice reflections of the same type for synthetic Mg-Al phases with an atomic ratio near 2:1. Taylor (1969) reported the existence of this sort of superstructure in sjögrenite, a natural mineral with composition close to $Mg_{2/3}Fe_{1/3}(OH)_2(CO_3)_{1/6}(H_2O)_{0.4}$. Bish (1977) also observed such a superstructure in a nickel aluminum hydroxycarbonate of the pyroaurite group, with observed unit-cell parameters close to those of hydrotalcite. In all these materials the superstructure corresponds to a molar R^{2+}:R^{3+} ratio of 2:1.

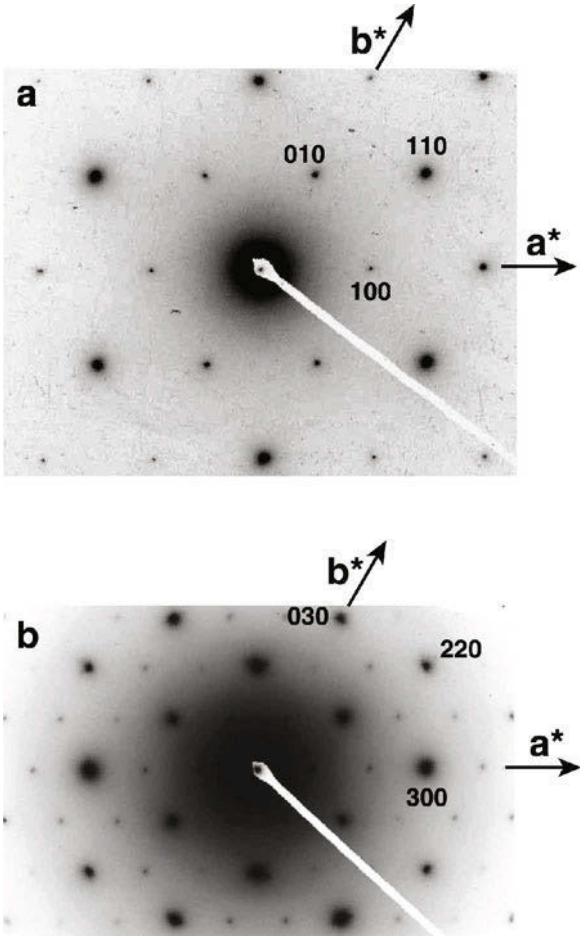

Figure 4. SAED patterns corresponding to (a) the classical hexagonal symmetry with a = 3.06 Å (Snarum, S1 and S2 synthetic samples) and to (b) superlattice hexagonal symmetry with a = 5.32 Å (few crystals in S1 synthetic sample).

Synthetic sample S2. Figure 2c includes the XRD pattern of sample S2. It is very different from those of samples N1 and S1. For sample N1 (Figure 2a), a segregation of rhombohedral hydrotalcite and hexagonal manasseite minerals was observed, and sharp reflections indicated the absence of stacking faults in the plane of the layers. For sample S1 (Figure 2b), our analysis of the hydrotalcite diffraction pattern shows a good crystallinity.

However, for sample S2 a significant disorder in layer stacking was recognized. General X-ray reflections (Figure 2c) were recorded from randomly oriented powders, but were not defined sufficiently well to provide unique indexing. A prominent reflection with a spacing of 1.531 Å, however, can be indexed as 110 with respect to hexagonal axes and with l = 0; this reflection is not dependent on the layer stacking arrangement. Parameter a (equal to parameter b) is twice d_{110}, *i.e.* 3.06_2 Å. The electron diffraction diagrams for this synthetic sample show patterns similar to that for the

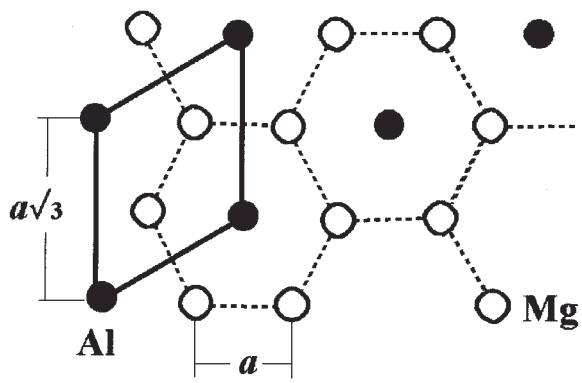

Figure 5. Possible distribution of Mg ions (open circles) and Al ions (solid circles) in octahedral sheet structure Mg:Al = 2:1 (Brindley and Kikkawa, 1979).

https://doi.org/10.1346/CCMN.2003.0510201 Published online by Cambridge University Press

natural sample from Snarum and a hexagonal symmetry in the *ab* plane. Indexing the cell with respect to hexagonal axes leads to a value of 3.08_3 Å for the *a* and *b* parameters. This sample shows stacking faults in the broad and asymmetric 01*l* reflections (Figure 2c). Bellotto *et al.* (1996) reported a powder XRD pattern of similar appearance for an experimental Mg/Ga hydrotalcite. The faults are a result of the interstratification of the rhombohedral and hexagonal polytypes. We can state that the powder XRD pattern of sample S2 is reminiscent of the material reported by Bellotto *et al.* (1996) to contain a random sequence of rhombohedral and hexagonal stacking. In summary, sample N1 presents a segregation of layers of hydrotalcite and manasseite minerals, with an absence of random stacking faults in the plane of the layers. Sample S1 presents a stacking mode corresponding to the $3R_1$ polytype. Sample S2 can be described as a random sequence of $3R_1$ and $2H_1$ polytypes.

Composition ranges of Mg,Al and unit-cell parameters

The proportions of Al in the natural and synthetic samples studied here are represented by Mg:Al ratios of 3:1 (N1 sample) and 3:1 and 2:1 (S2 and S1, respectively). The unit-cell parameters of the samples can be related to the octahedral charge and to the cation radius, as shown in Figure 6. Brindley and Kikkawa (1979) and Bellotto *et al.* (1996) noted similar phenomena. The layer spacing *c* and the hexagonal *a* parameter diminish as layer charge increases, the former because of increasing electrostatic attraction, the latter because of the smaller size of the Al^{3+} ions.

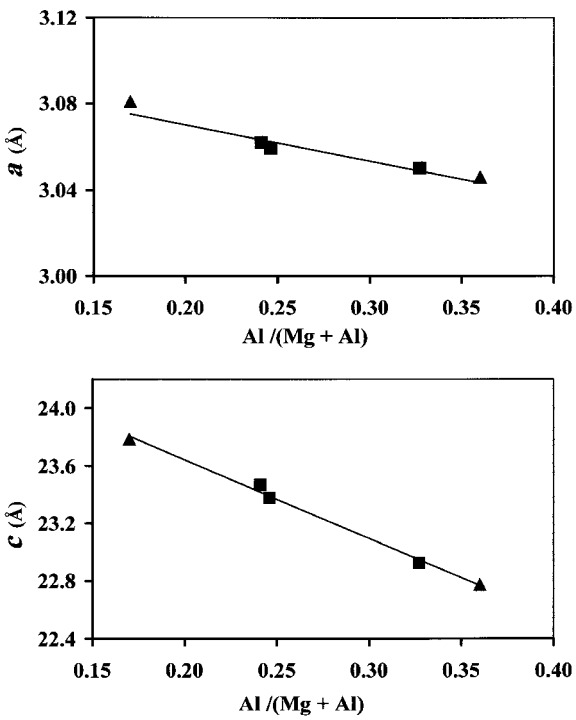

Figure 6. Correlation between *a* and *c* parameters *vs.* Al/(Mg+Al) ratio. ■ N1, S1, S2 samples, ▲ Bellotto *et al.* (1996).

Texture: SEM and TEM

Sample from Snarum. The electron micrographs obtained for the green portion (serpentine) of the sample are shown in Figure 7a. There is a distinct layered structure, with weakly developed layers in the lateral direction. The structure and the morphology are planar as in most lizardites, in amesite, and in other aluminian serpentine minerals. A qualitative SEM analysis shows that the main elements forming this mineral are Si, Mg, Al and O. Random spot analyses show an homogeneous distribution of these cations in this material. The *x* substitution for the composition $(Mg_{3-x}Al_x)(Si_{2-x}Al_x)O_5(OH)_4$ of Al for Mg and Si is near 1, in agreement with Gillery's results for a 6-layer lizardite structure (see Table 2). A small amount of Fe and Zr were also detected. Caillère (1946) reported the presence of hematite and titaniferous magnetite impurities in serpentine deposits in Snarum.

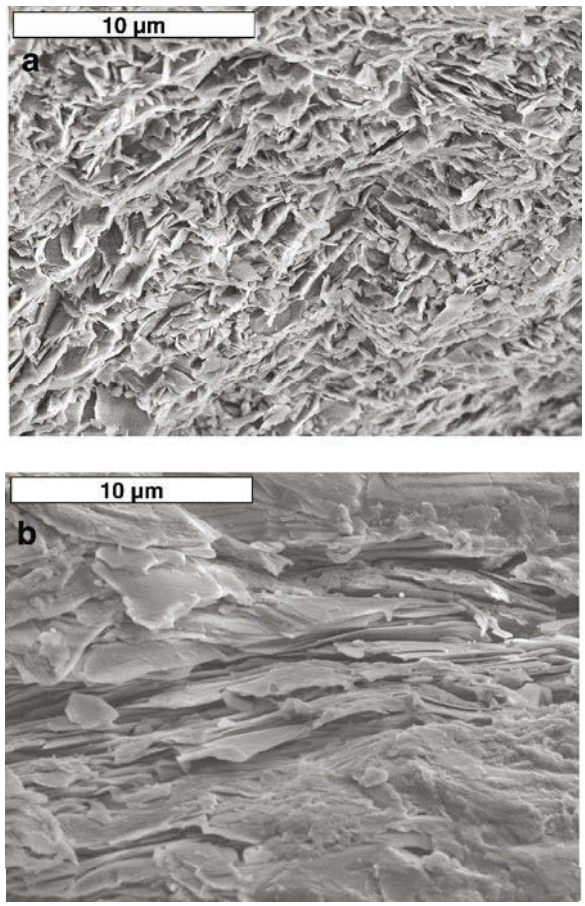

Figure 7. SEM images of the natural sample from Snarum: (a) green part (serpentine), (b) white part (hydrotalcite + manasseite).

https://doi.org/10.1346/CCMN.2003.0510201 Published online by Cambridge University Press

Figure 7b shows SEM images of the white portion of the Snarum sample (hydrotalcite, manasseite). The morphology observed is typical of layered minerals, with thin, platey crystals and overlapping of layer stacks. The SEM qualitative elemental analysis was made on polished cuts showing C, Al, Mg and O ions. The EDS mapping obtained shows an homogeneous distribution of these elements.

The electron micrographs obtained by TEM on well dispersed fragments of the white part of this sample show pseudohexagonal symmetry with dimensions of 3–8 μm. The images of the green part show a more pronounced hexagonal morphology, with a size close to 0.5 μm.

Synthetic sample S1. Figure 8a shows the images obtained for this sample, indicating an overlapping of small hexagonal crystals with dimensions close to 0.5 μm. The analysis performed with the analytical SEM confirms the presence of C, Al, Mg and O, with an homogeneous distribution, according to EDS mapping.

Synthetic sample S2. Figure 8b shows SEM images of this sample, with small stacks of layers formed by hexagonal planar, thin platelets. The size of the crystals in the direction of the plane is 1–3 μm, larger than that measured for crystals of sample S1. Analysis by SEM confirmed the existence of homogeneously distributed elements characteristic of hydrotalcite. As for previous samples, EDS mapping showed an homogeneous distribution of the main elements. The Mg:Al ratio is clearly greater than in sample S1, as shown by the atomic absorption results.

In dispersed crystals of this sample, well defined hexagonal planar platelets can be observed (TEM), whose sizes range from 0.5 to 2 μm, most of the crystals showing a size of 1.5 μm.

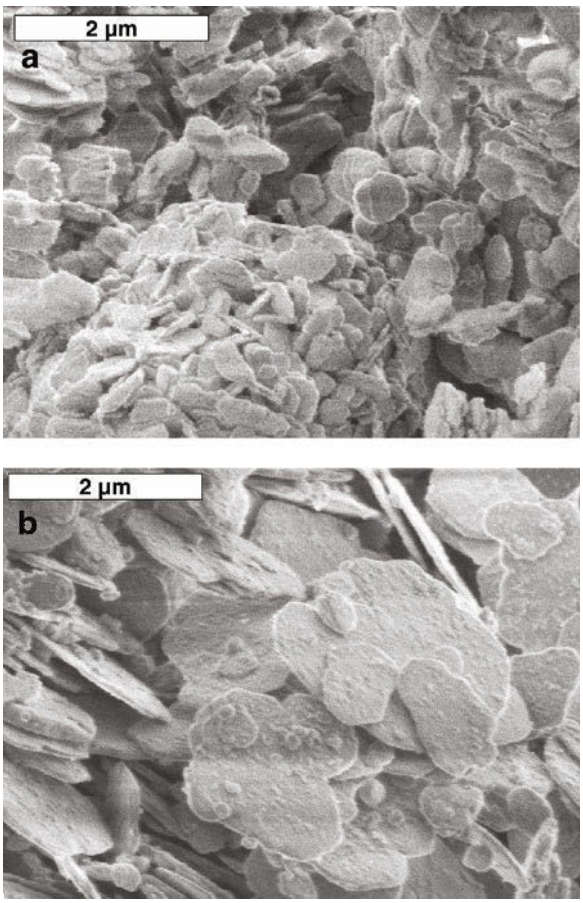

Figure 8. SEM images of S1 (a) and S2 (b) synthetic samples.

DISCUSSION AND CONCLUSIONS

The proportions of Al in the natural and synthetic samples studied here are represented by Mg:Al ratios of 3:1 (N1 sample) and 3:1 and 2:1 (for the S2 and S1 samples, respectively). The unit-cell parameters of the samples and the brucite-like sheet thickness can be related to the octahedral charge as shown in Figure 6. There is a good correlation between our results and those obtained by Bellotto (1996).

X-ray diffraction data show that the Snarum sample, N1, is an intergrowth of 77 wt.% hydrotalcite ($3R_1$ polytype) and 23 wt.% manasseite ($2H_1$ polytype). An aluminian serpentine termed 6(3)-lizardite is associated with N1. The S1 structure was determined with space group $R\bar{3}m$. S2 was described as a random layer sequence of two polytypes ($3R$ and $2H$).

The XRD analysis of hydrotalcite-like minerals by Rebours *et al.* (1994) and Bellotto *et al.* (1996) revealed $R\bar{3}m$ ordered hydrotalcite-like structures in samples of composition with Mg:Al = 1.8; 2; 4.8; and 5 as in our sample S1 (2:1 ratio). Disordered structures appear in synthetic samples with an Mg:Al ratio near 3, as in sample S2. In the natural sample, N1, with Mg:Al = 3, ordered structures of two polytypes $3R$ and $2H$ are present. A hexagonal phase accompanying a rhombohedral phase only appears when the proportion of Al within the brucitic sheet is close to 25 wt.%.

A correlation seems to exist between the chemical composition and the structural arrangement among the layers. For the synthetic samples, coprecipitation at the same temperature as the surroundings seems to create conditions favorable to the formation of hydrotalcite. Nevertheless, the results show that the Mg/Al ratio is an important factor too. At a critical value (Mg:Al = 3), a disordered structure, linked to stacking faults due to interstratification between $2H$ and $3R$ polytypes, appears. The random nature of the distribution of the two polytypes within the stack might be explained by the principle of coprecipitation and by the fact that there is no supplementary energy input from the surroundings. To explain the segregation of manasseite and hydrotalcite observed in the natural samples with an Mg:Al ratio close to three it might be necessary to consider the

https://doi.org/10.1346/CCMN.2003.0510201 Published online by Cambridge University Press

cooling rate during the formation of particles. To do this, it is first necessary to recall that the rhombohedral three-double-layer crystal with P-type interlayers, represented by the sequence ...AC=CB=BA=AC... (Bookin and Drits, 1993) can be described from a unique brucite-like sheet AC; three translations between consecutive layers AC of ($2a/3+b/3$) describe the 3*R* polytype. In the same way, the hexagonal two-double-layer polytype ...AC=CA=AC... can be described from the AC brucite-like sheet with a translation of ($2a/3+b/3$) and then a 60º rotation. The rotation of the sheets, necessary to form the hexagonal polytype from a single type of sheet, requires higher temperatures than the rhombohedral polytype, for which only translations between the sheets are needed. This would be in agreement with the fact that, for an Mg:Al ratio of 3 in natural samples, the formation of manasseite is observed at higher temperatures than is the case for hydrotalcite formation.

During formation, the outer part of the grain cools more rapidly, which would be compatible with the formation of the 3*R* polytype, which consists entirely of translations of the layers.

The higher temperature maintained within the grains over a longer period would permit the 60º rotations of the layers required for the formation of the 2*H* polytype.

Thus, the formation of the 2*H* polytype in the N1 sample might depend not only on the thermodynamic but also on kinetic factors and the Mg:Al ratio.

ACKNOWLEDGMENTS

This work is dedicated to the beloved memory of Dr Maria Angeles Vicente (deceased April 28th, 2000). We are grateful to Mr Jalabert and Mrs Richard for the electron microscopy experiments. Comments by reviewers are gratefully acknowledged. V.R. acknowledges financial support from MCyT (grant MAT2000-1148-C02-01).

REFERENCES

Allman, R. and Lohse, H.H. (1966) Die Kristallstruktur des Sjögrenits und eines Umwandlungs produktes des Koenenits (=chlor-Manasseits). *Neues Jahrbuch für Mineralogie Monatshefte*, 161–181.

Arakcheeva, A.V., Pushcharovskii, D.Yu., Rastsvetaeva, R.K., Atencio, D. and Lubman, G.U. (1996) Crystal structure and comparative crystal chemistry of $Al_2Mg_4(OH)_{12}CO_3.3H_2O$, a new mineral from the hydrotalcite-manasseite group. *Crystallography Reports,* **41**, 972–981.

Bailey, S.W. and Tyler, S.A. (1960) Clay minerals associated with the Lake Superior iron ores. *Economic Geology and the Bulletin of the Society of Economic Geologists,* **55**, 150–175.

Bellotto, M., Rebours, B., Clause, O., Lynch, J., Bazin, D. and Elkaïm, E. (1996) A reexamination of hydrotalcite crystal chemistry. *Journal of Physical Chemistry B*, **100**, 8527–8534.

Bish, D.L. (1977) The occurrence and crystal chemistry of nickel in silicate and hydroxide minerals. Ph.D. thesis, Pennsylvania State University, University Park, Pennsylvania, USA.

Bookin, A.S. and Drits, V.A. (1993) Polytype diversity of the hydrotalcite-like minerals I. Possible polytypes and their diffraction features. *Clays and Clay Minerals,* **41**, 551–557.

Brindley, G.W. (1980) Order-disorder in clay mineral structures. Pp. 125–196 in: *Crystal Structures of Clay Minerals and their X-ray Identification* (G.W. Brindley and G. Brown, editors). Monograph **5**, Mineralogical Society, London.

Brindley, G.W. and Kikkawa, S. (1979) A crystal study of Mg, Al and Ni, Al hydroxy-perchlorates and hydroxy-carbonates. *American Mineralogist,* **64**, 836–843.

Caillère, S. (1946) Etude microscopique de quelques minéraux opaques associés à la serpentine de Snarum (Norvège). *Société française de Mineralogie,* **B 69**, 1–12, 51–55.

Cavani, F., Trifirò, F. and Vaccari, A. (1991) Hydrotalcite-type anionic clays: preparation, properties and applications. *Catalysis Today*, **11**, 173–301.

de la Calle, C., Suquet, H. and Pons, C.H. (1988) Stacking order in a 14.30 Å Mg-vermiculite. *Clays and Clay Minerals,* **36**,481–490.

Drits, V.A. and Tchoubar, C. (1990) *X-ray Diffraction by Disordered Lamellar Structures*. Springer-Verlag, Berlin, Heidelberg, 371 pp.

Feitknecht, W. (1930) Untersuchungen über die Umsetzung fester Stoffe in Flüssigkeiten. 1. Mitteilung: Über einege basische Zinksalze. *Helvetica Chimica Acta,* **13**, 22–43.

Feitknecht, W. (1953) Die fasten Hydroxisalzen zweiwertiger Metalle. *Fortschritte der Chemischen Forschung,* **2**, 670–757.

Frondel, C. (1941) Constitution and polymorphism of the pyroaurite and sjögrenite groups. *American Mineralogist,* **26**, 295–303.

Gastuche, M.C., Brown, G. and Mortland, M.M. (1967) Mixed magnesium-aluminium hydroxides. I. Preparation and characterization of compounds formed in dialyzed systems. *Clay Minerals,* **7**, 177–192.

Gillery, F.H. (1959) The X ray study of synthetic Mg-Al serpentines and chlorites. *American Mineralogist,* **44**,143–152.

Hunter, B.A. and Howard, C.J. (2000) *A computer program for Rietveld analysis of X-ray and neutron powder diffraction patterns*. Lucas Heights Research Laboratories, Private Mailbag 1, Menai 2234, New South Wales, Australia.

Pausch, H., Lohse, H., Schürmann, K. and Allman, R. (1986) Synthesis of disordered and Al-rich hydrotalcite-like compounds. *Clays and Clay Minerals*, **34**, 507–510.

Raade, G. (1970) Dypingite, a new hydrous basic carbonate of magnesium, from Norway. *American Mineralogist,* **55**, 1457–1465.

Rebours, B., Espinose de la Caillère, J.B. and Clause, O. (1994) Decoration of nickel and magnesium oxide cristallites with spinel-type phases. *Journal of the American Chemical Society*, **116**, 1707–1717.

Rives, V. and Ulibarri, M.A. (1999) Layered double hydroxides (LDH) intercalated with metal coordination compounds and oxometalates. *Coordination Chemistry Reviews,* **181**, 61–120.

Roux, J. and Volfinger, M. (1996) Mesures précises à l'aide d'un détecteur courbe. *Journal de Physique,* VI, C4, **6**, 127–134.

Roy, D.M., Roy, R. and Osborn, E.F. (1953) The system MgO-Al_2O_3-H_2O and influence of carbonate and nitrate ions on the phase equilibria. *American Journal of Science,* **251**, 337–361.

Roy, A. de, Forano, C., Khaldi, M., El Malki, K. and Besse, J.P. (1992) Expanded clays and other microporous solids. Pp. 108–169 in: *Synthesis of Microporous Systems* (M.L. Occelli and H.E. Robson, editors). Van Nostrand Reinhold, New York.

Shirozu, H. and Momoi, H. (1972) Synthetic Mg-chlorite in relation to natural chlorite. *Mineralogical Clay Journal,*

Sapporo, **6**, 464–476.

Szostak, R. and Ingram, C. (1995) Pillared layered structures (PLS). Pp. 13–38 in: *Catalysis by Microporous Materials* (H.K. Beyer, H.G. Karge, I. Kiricsi and J.B. Nagy, editors). Studies in Surface Science and Catalysis, **94**, Elsevier, Amsterdam.

Taylor, H.F.W. (1969) Segregation and cation ordering in sjögrenite and pyroaurite. *Mineralogical Magazine,* **37**, 338–389.

(*Received 28 November 2001; revised 18 November 2002; Ms. 609; A.E. Peter J. Heaney*)